Systematic Investigations of Fatigue Crack Growth Behavior of a PE-HD Pipe Grade in Through-Thickness Direction

W. Balika,[1] G. Pinter,[2] R. W. Lang[1,2]

[1]*Polymer Competence Center Leoben GmbH (PCCL), Parkstrasse 11, A-8700 Leoben, Austria*
[2]*Institute of Materials Science and Testing of Plastics, University of Leoben, Franz-Josef-Strasse 18, A-8700 Leoben, Austria*

Received 5 April 2006; accepted 20 June 2006
DOI 10.1002/app.25073
Published online in Wiley InterScience (www.interscience.wiley.com).

ABSTRACT: Fatigue crack growth (FCG) experiments were performed on a commercial high-density polyethylene (PE-HD) pipe grade. To investigate the influence of different specimen types on FCG results, tests were conducted using compact tension (CT) specimens and cracked round bars (CRB). The effects of frequency and R-ratio on FCG behavior were also studied. Furthermore, FCG tests were interrupted in the region of stable crack propagation. The crack front and the front of the process zone ahead of the crack were systematically characterized via microscopic methods in the thickness direction of the specimen. The experimental data are employed to study the mechanisms of process zone development and to determine the effective crack length by compliance relationships. This detailed information allows modeling FCG in PE-HD at various positions in the thickness direction of the specimen. © 2006 Wiley Periodicals, Inc. J Appl Polym Sci 103: 1745–1758, 2007

Key words: polyethylene; fatigue; crack growth; process zone; through-thickness characterization

INTRODUCTION AND OBJECTIVES

It is well known that an understanding of the creep crack growth (CCG) phenomenon is one of the most important factors in the evaluation of the long-term performance of thermoplastic pipes. It is generally acknowledged that the origin of this phenomenon is the formation, growth, and failure of plastic zones at places of stress concentration. Although in the literature the resistance to crack propagation is attributed predominantly to the phenomenon of chain disentanglement, there are enough indications that chain fracture plays an important role in this context.[1–3] Specifically, newer investigations by Lang and Pinter[4–6] on polyethylene (PE) have strengthened the hypothesis that local crack tip aging processes affect the kinetics of crack propagation. Contrary to the belief that the density of tie chains connecting adjacent crystalline lamellas predominantly determines the lifetime of PE pipes, there are currently some attempts to correlate the degree of mobility of the amorphous phase to failure times measured in PE pipe materials.[7]

It is well established that quasi-brittle failure consisting of crack initiation and crack propagation can be realized in principle under laboratory conditions by various mechanical approaches. In regard to a reduction of testing time, the main principle of all concepts is to tighten significant test parameters such as temperature, applied stress, environmental condition (surfactants), and loading condition.[8–13] Owing to the complexity of the failure and aging mechanisms, which all strongly depend on time and temperature, there are still some limitations to the applicability of these test data for a flawless lifetime prediction of thermoplastics pipes under real service conditions.[4,8,12,14,15]

Despite the basic difference in loading conditions, some research groups favor fatigue test approaches in evaluating new pipe grades and in evaluating the long-term performance under constant loading conditions for the following reasons. First, fatigue loading principally leads to accelerated crack growth. Second, similar characteristics have been found in creep crack growth and fatigue crack growth (FCG) in various PE materials.[16–20]

Many fatigue investigations on PE, based on cyclical pressurized pipe tests[17,21,22] and fracture mechanics methods[20,23–25] have shown that FCG in PE occurs either by a quasi-continuous mechanism or by a discontinuous (stepwise) mechanism. As different work groups[24,26] have shown, the crack growth mode depends on various test parameters such as the R-ratio (minimum to maximum load), test temperature and the stress level.

Correspondence to: W. Balika (balika@pccl.at).
Contract grant sponsors: Austrian Government; State Governments of Styria and Upper Austria.

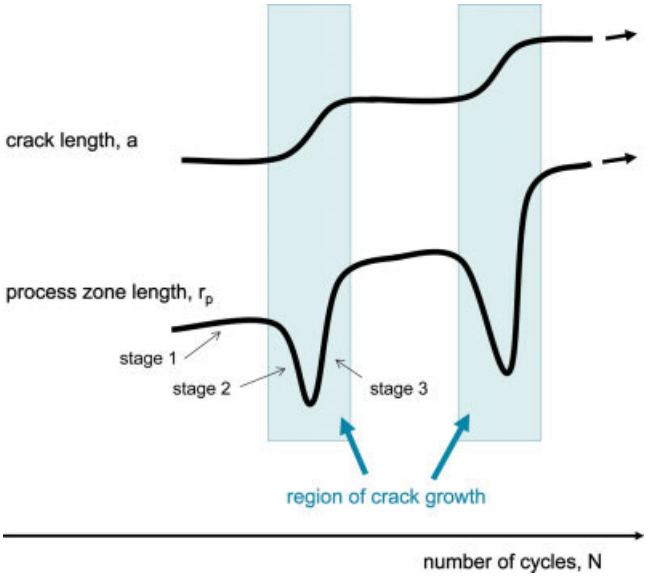

Figure 1 Schematic representation of phenomenological model for discontinuous crack growth. [Color figure can be viewed in the online issue, which is available at www.interscience.wiley.com.]

Discontinuous crack growth in PE occurs by sequential formation and failure of the process zone in front of the crack tip. A possible phenomenological model in terms of crack length, a, and process zone length, r_p, is shown in Figure 1. The process zone, which consists of highly fibrillated and stretched material, develops continuously in front of the crack tip, as illustrated by the increasing r_p-values (stage 1). Simultaneously, the crack is arrested until the fibrils deteriorate enough for the process zone to break down and the crack jumps through the process zone. At that point in time, which normally happens within a few thousands cycles, the crack length increases significantly, while the process zone length decreases (stage 2). Depending on the test parameters, both step jumps through the entire process zone and step jumps through a part of the process zone were observed.[24] Because of the relatively quick formation of a larger process zone ahead of the crack tip (stage 3), the crack is arrested again and the phenomena repeat. In summary, the phenomenological model presented splits discontinuous crack growth into three stages. The region of crack growth includes the stages 2 and 3.

The main objective of the research reported here was (1) to characterize the FCG in a high-density polyethylene (PE-HD) pipe grade using a method based on a linear elastic fracture mechanics (LEFM) approach and (2) to examine the development of the crack front and the front of the process zone ahead of the crack in the thickness direction of the specimen during the fatigue tests. In contrast to research reported in the literature, the novelty of this work was the determination of a very dense array of data points in the through-thickness direction. The effects of specimen configuration, stress intensity factor, frequency, and R-ratio were investigated systematically. The experimental data were determined to study the mechanisms of FCG and process zone development and to calculate the effective crack length based on compliance relationships. Furthermore, the information gained from these investigations should be used to develop and implement a methodology for modeling FCG in PE-HD at various positions in the thickness direction of the specimen.

EXPERIMENTAL

All investigations reported in the present study were performed on a commercial, carbon-filled PE-HD pipe grade (DOW Chemical, CH), classified as PE100 material. Throughout this report, it is labeled as PE100-1.

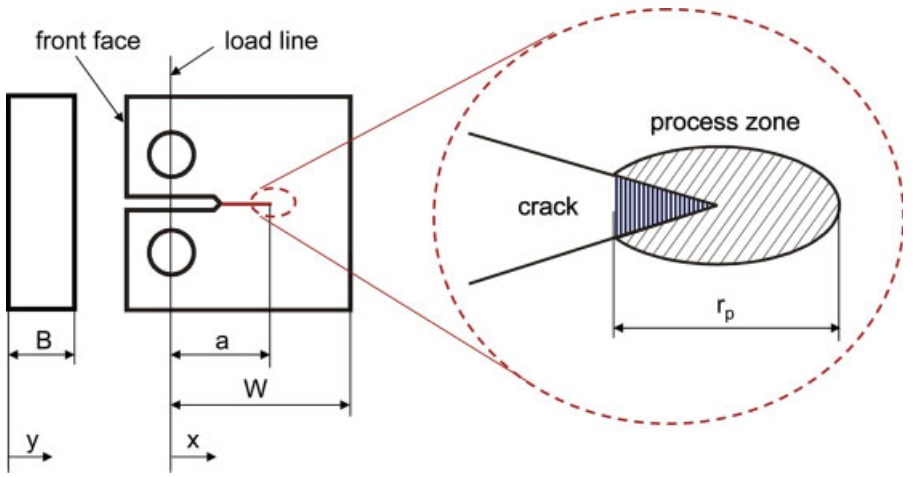

Figure 2 Schematic representation of characteristic dimensions of a CT specimen and process zone ahead of the crack. [Color figure can be viewed in the online issue, which is available at www.interscience.wiley.com.]

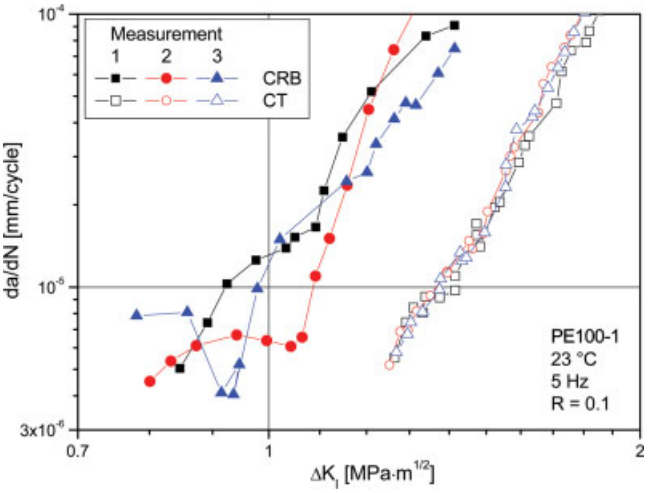

Figure 3 FCG rates in PE100-1 as a function of ΔK_I, using CT and CRB specimens (23°C, 5 Hz, R = 0.1). [Color figure can be viewed in the online issue, which is available at www.interscience.wiley.com.]

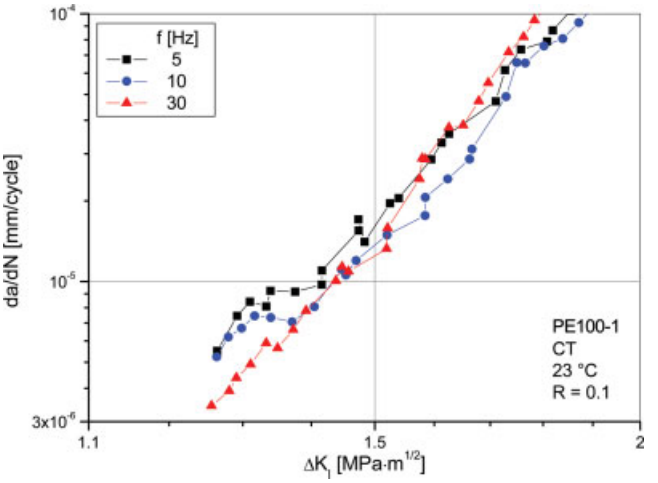

Figure 4 FCG rates as a function of ΔK_I in PE100-1 using CT and CRB specimens at various frequencies (23°C, R = 0.1). [Color figure can be viewed in the online issue, which is available at www.interscience.wiley.com.]

Compact tension (CT) specimens with a width, W, of 40 mm and a thickness, B, of 15 mm and cracked round bars (CRB) with a length, L, of 100 mm and a diameter, D, of 14 mm were machined from 15-mm-thick compression-molded plaques. Razor blades were used for pre-cracking the specimens.

Based on the concepts of LEFM, the FCG tests were performed using a servo-hydraulic closed-loop testing machine (MTS System GmbH, Berlin, D) under sinusoidal load control at frequencies of 5, 10, and 30 Hz and with R-ratios of 0.1, 0.3, and 0.5. The tests were carried out in air at room temperature (23°C) and at a relative humidity of 50%.

Using CT specimens, additional FCG tests for each parameter set were interrupted in the region of stable crack propagation at three different values of stress intensity factor, $\Delta K_{I,int.}$. The region of stage 1 illustrated in Figure 1 was of particular interest for the through-thickness characterization of the process zone. To stabilize and preserve the crack formed at the maximum stress intensity factor at the interruption point ($K_{Imax,int}$), the interrupted cracks were filled with a commercial epoxy resin. Crack profiles, including the process zone, were laid open in the thickness direction of the CT specimen using a microtome cutting technique. Both crack and process zone were measured using optical methods (Fig. 2).

RESULTS AND DISCUSSION

FCG kinetics

To investigate the effect of specimen configuration on FCG, fatigue tests were conducted using CT and CRB specimens of PE100-1 at 5 Hz and an R-ratio of 0.1. The main reason for selecting CRB specimens was the well-defined plane strain condition in the ligament. In Figure 3, FCG curves are compared for three different CRB and CT specimens of PE100-1. Since asymmetric crack propagation was found in the most cases of CRB testing, the ΔK_I values calculated for CRB specimens represent some kind of average values. It is obvious that the scatter in the results is much higher for the CRB specimens. This can be explained in two ways. On the one hand, asymmetric crack growth makes it very difficult to identify the right crack length. In contrast, the high gradient of ΔK_I in these load-controlled tests (with constant load peaks) makes the generation of FCG data rather difficult. Moreover, it is obvious from Figure 3 that the FCG data from the CRB speci-

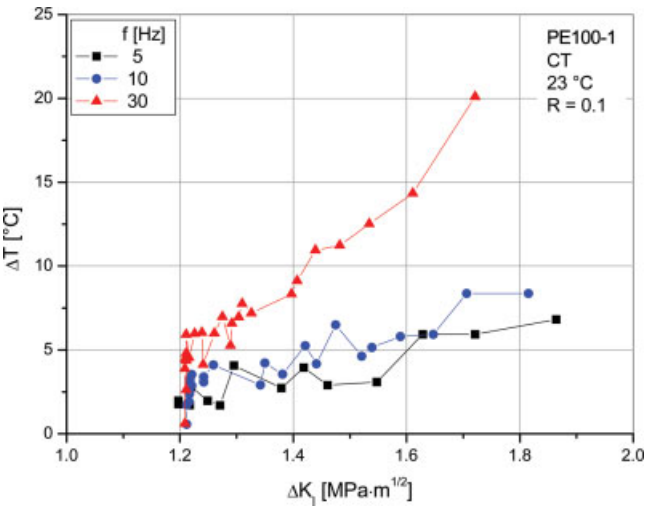

Figure 5 Temperature rise at the crack tip as a function of ΔK_I (CT, 23°C, R = 0.1, ΔK_{I0} = 1.2 MPa·m$^{1/2}$). [Color figure can be viewed in the online issue, which is available at www.interscience.wiley.com.]

mens is shifted to higher crack growth rates. Based on LEFM, FCG should be independent of the specimens used. Apparently, the pronounced plane strain conditions in CRB specimens are responsible for the decrease in FCG resistance compared with CT specimens, where plane stress conditions prevail at least at the specimen surfaces. Furthermore, more investigations will be necessary to clarify the possible influence of asymmetric crack propagation on the differences in kinetic data.

The effect of frequency on FCG behavior will be obvious from Figure 4, which compares the kinetic results of fatigue tests conducted at 5, 10, and 30 Hz, using CT specimens of PE100-1. It becomes apparent that with increasing test frequency there is a noticeable increase in crack growth resistance in CT specimens in the low crack-growth regime. At higher crack-growth rates, the curves coincide. This frequency sensitivity of FCG in polymers can be explained in terms of the effects of changes in strain rate on the dynamic modulus and by the effects of localized heating, which blunts the crack tip (beneficial), versus generalized heating, which leads to an overall decrease in specimen stiffness (detrimental).[27,28] In the low ΔK_I range, a higher frequency leads to lower crack growth rates because of the higher dynamic modulus of the material under these test conditions and the enhanced crack-tip blunting due to increased localized heating. The coinciding curves at higher ΔK_I values can be interpreted in terms of the increasing importance of a modulus drop due to cross-specimen heating at higher test frequencies and resulting in higher crack growth rates. Thus, due to the importance of other factors affecting possible changes in FCG rate with frequency (local strain rate, loading rate, area under force–time curve, creep

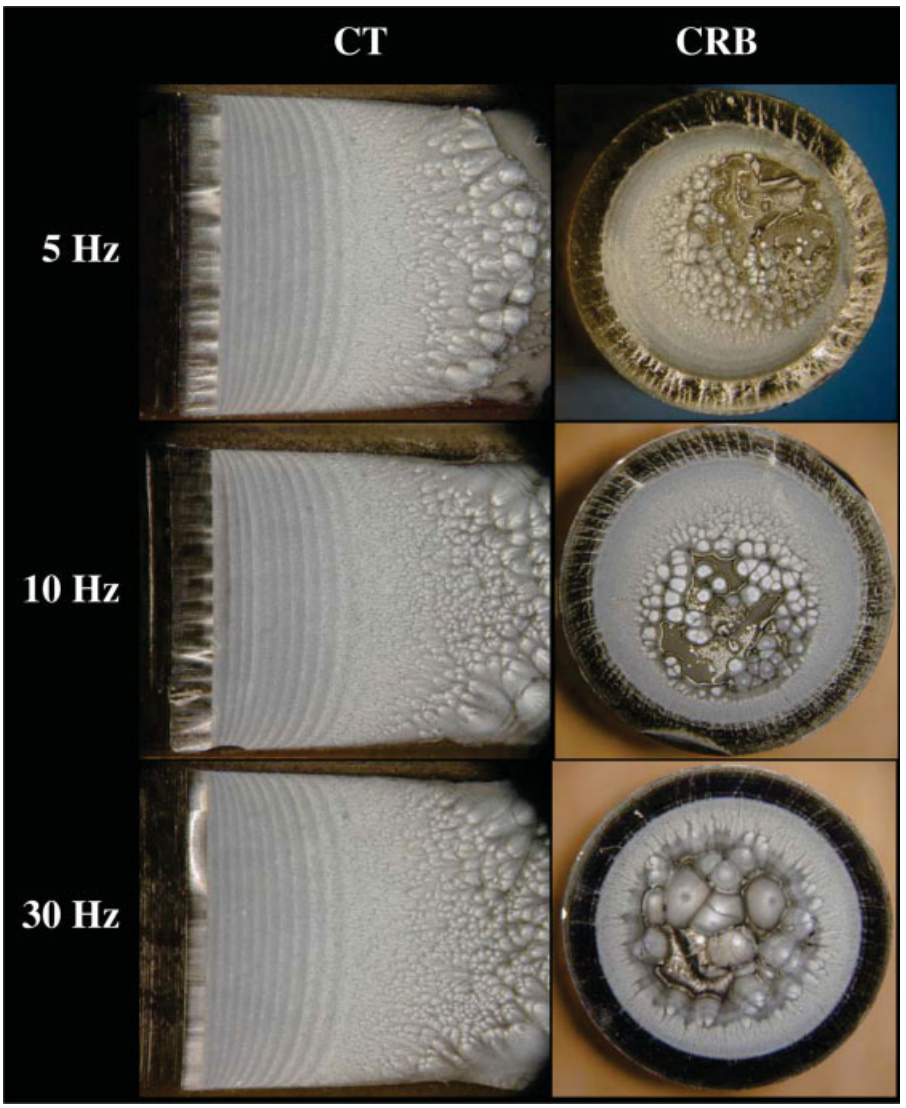

Figure 6 Optical photos of PE100-1 after testing at various frequencies (23°C, R = 0.1). [Color figure can be viewed in the online issue, which is available at www.interscience.wiley.com.]

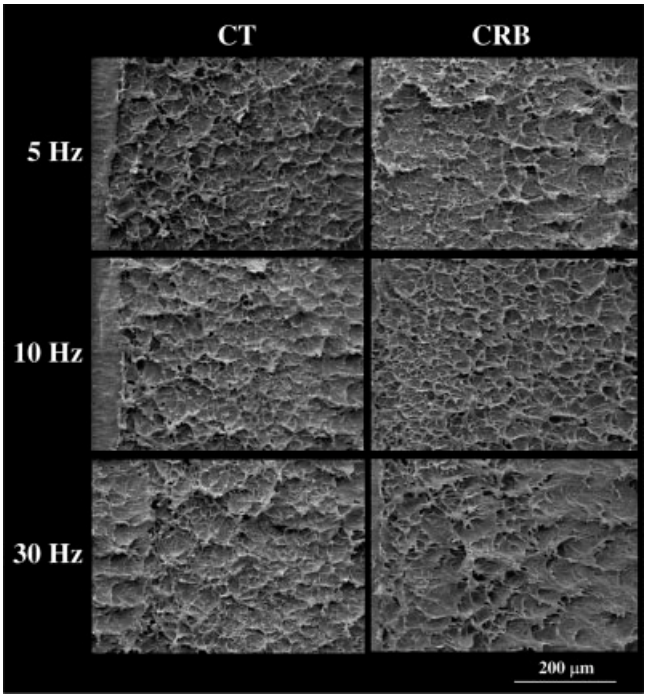

Figure 7 SEM photos of PE100-1 after testing at various frequencies (23°C, R = 0.1).

effects[27,28]), the behavior observed at higher FCG rates in Figure 4 can be explained by a compensation of all conflicting processes.

For all three frequencies investigated, the temperature increase, ΔT, at the crack tip was measured using an infrared camera (Cedip Infrared Systems, Croissy Beaubourg, France) for the CT specimen (Fig. 5). Similar increases in temperature at the crack tip from approximately 2°C after crack initiation to 7°C within the relevant ΔK_I range occurred at both 5 and 10 Hz. At 30 Hz, crack-tip heating was distinctly increased with temperatures from 5°C to about 20°C. In addition, the temperature rise was measured at another two positions in the CT specimen for 5, 10, and 30 Hz: (1) close to the crack tip, and (2) far away from the crack tip where (almost) no hysteretic heating was assumed. While a small temperature increase up to ~3°C was observed close to the crack tip for frequencies of 5 and 10 Hz, significantly higher changes of temperature in the range of 3–8°C occurred at 30 Hz. For all frequencies investigated (almost) no increase in temperature occurred at the position far away from the crack tip.

In addition to the CT specimen, CRB was also used to study the effect of frequency on FCG behavior. Typical fracture surfaces of specimens tested at the different frequencies are compared in Figure 6. For the CT specimens, striations on the fracture surfaces document the stepwise crack growth mechanism at all frequencies. No clear differences in the details of the fracture surfaces could be found as a result of the variations in frequency. Asymmetric crack growth was commonly characteristic for the CRB tests. Striations could only be detected at 5 Hz. It was striking that the area of quasi-brittle crack propagation got smaller with increasing frequency. In the case of 30 Hz, predominantly ductile failure was observed, documented by the coarser and more blurred structures. This fact is assumed to be a result of increased hysteretic heating effects at the crack tip.

Details of the fracture surfaces were compared at the sites of crack initiation (Fig. 7). The fracture surface in the brittle failure regime of both specimen types is characterized by the typical attributes of craze formation and breakdown (voids and fibrils). In general, no significant differences in the details of the fracture surfaces could be found as a result of the different specimen configurations but structures on the fracture surface of the CRB specimens are finer because testing was started at lower initial values of stress intensity factor range, ΔK_{I0} (0.75 MPa·m$^{1/2}$ vs 1.2 MPa·m$^{1/2}$). A comparison at equal values of stress intensity factor was not possible here due to the phenomenon of asymmetric crack propagation in the CRB specimens. Although there have been some attempts to calculate ΔK_I for eccentric problems,[29] a proper solution is still missing.

The time to failure, t_f, was also documented and the results are presented in Table I. It is not surprising that test times were reduced at increased frequency. However, it must be borne in mind that the heating effects must be considered in all discussions of this aspect (cf. Fig. 5). Therefore, the test results are also presented as the number of cycles to failure, N_f. Compared with the tests carried out at 5 Hz, the N_f values significantly increased in the tests at 30 Hz. That is in good correlation with the kinetic data presented in Figure 4.

In comparison with CT testing, the main advantage of CRB testing was the reduction in testing time, which could be of particular interest when ranking of materials is the goal. Although the tests with CRB specimens were started at a lower initial stress intensity factor range than the tests with CT specimens, the

TABLE I
Time to Failure, t_f, and Number of Cycles to Failure, N_f, for FCG Investigations on PE100-1 at Various Frequencies Using CT and CRB Specimens (23°C, R = 0.1)

	f [Hz]	CT (ΔK_{I0} = 1.2 MPam$^{1/2}$)	CRB (ΔK_{I0} = 0.75 MPam$^{1/2}$)
t_f [h]	5	37.2	18.9
	10	21.5	9
	30	7.8	4.3
N_f	5	669,000	340,000
	10	774,000	324,000
	30	842,000	464,000

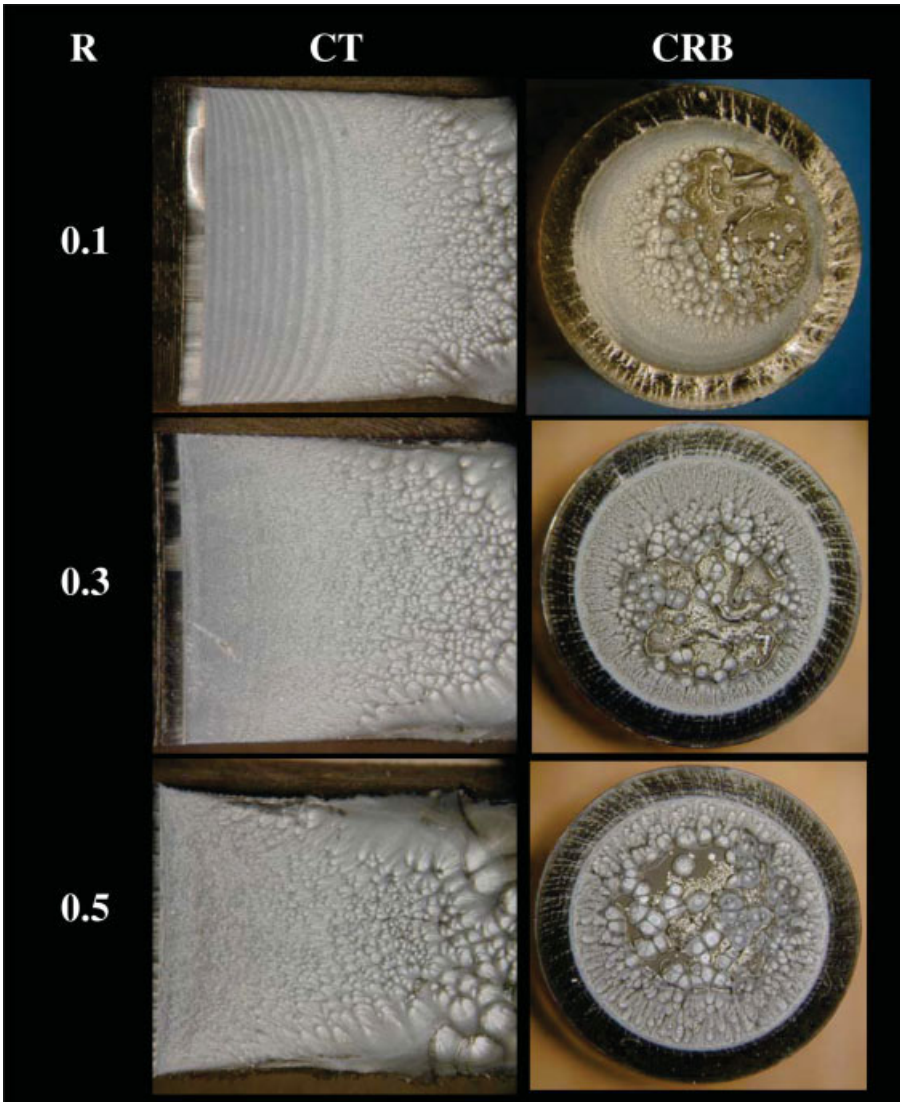

Figure 8 Optical photos of PE100-1 after testing at various R-ratios (23°C, 5 Hz).

testing times dropped to approximately one-half. It is interesting to note that the CRB testing methodology has been further developed and implemented as a powerful tool for material ranking.[30,31]

The pronounced influence of the R-ratio on the micromorphology of the fracture surface of the investigated PE is illustrated in Figures 8 and 9. As the initial values of the maximum stress intensity factor, $K_{Imax,0}$, were higher for the tests at higher R-ratios, there are more highly stretched fibrils as the R-ratio is increased. In all tests, and especially for CRB specimens, the fracture surfaces reflect a transformation from quasi-brittle failure to ductile failure with increasing R-ratio. It is important to note that under the test conditions selected here, there was a clear difference in the crack growth mechanism, which became visible during scanning electron microscopy (SEM) analysis of the fracture surface and analysis of crack opening displacement (COD) data. While an R-ratio of 0.1 lead to a discontinuous crack propagation characterized by the expected striations on the fracture surface, these features became increasingly indistinct at an R-ratio of 0.3, indicating a change of crack growth mode from discontinuous to continuous crack propagation.

FCG data for PE100-1, illustrating the effects of variations in R-ratio at a given frequency (5 Hz) for CT specimens, are shown as a function of the applied stress intensity factor range and the maximum stress intensity factor in Figure 10. In terms of ΔK_I, the FCG rates were found to strongly depend on the R-ratio. In the case of $R = 0.5$, the validity of LEFM was limited to low da/dN-values and low ΔK_I-values. Since a shift of the curve to the left was observed with increasing R-ratio, FCG rates in PE100-1 are controlled not only by the stress intensity factor range at the defined test parameters, but also by the maximum stress intensity factor and/or the mean stress intensity factor, which

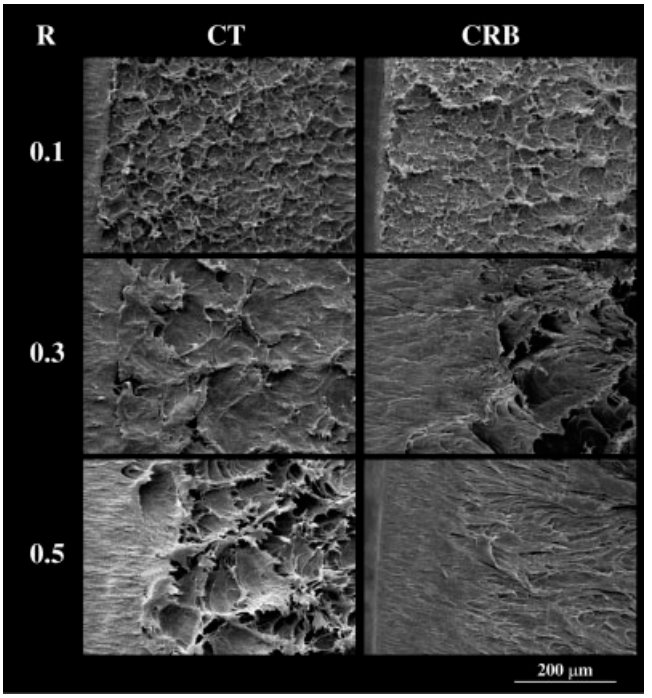

Figure 9 SEM photos of PE100-1 in the region of crack initiation after testing at various R-ratios (23°C, 5 Hz).

is in good agreement with previously reported results.[19,28,32,33] There may be a tendency for higher crack growth rates at higher R-ratios as a result of more creep crack extension associated with the higher maximum and mean stress intensity levels.[19,34]

While no kinetic data were determined for CRB due to the asymmetric crack growth phenomenon, the time to failure, t_f, were also documented for all tests at various R-ratios. The results are presented in Table II, including detailed information to the initial values of stress intensity factor (ΔK_{I0} and $K_{Imax,0}$). In the case of CT specimens, the testing times were in the range of 37 to 44 h. In the tests in which quasi-brittle crack propagation was achieved (R = 0.1 and partly R = 0.3), the CRB specimens failed after ~20 h, whereas ductile failure occurred after just 1 h (R = 0.5).

Process zone characterization

Research groups dealing with the subject of local phenomena at crack tips in thermoplastic pipe grades often concentrate their investigations on process zone size measurements at the side surface and/or in the middle of the specimens.[23,35] More information could be gained, if the distribution of process zone size through the whole thickness of the specimen were known. The results of such investigations on PE100-1 are shown in Figures 11 and 12. The FCG tests at 23°C, an R-ratio of 0.1 and a frequency of 5 Hz were interrupted at ΔK_I values of 1.6 MPa·m$^{1/2}$ (Fig. 11) and 1.4 MPa·m$^{1/2}$ (Fig. 12).

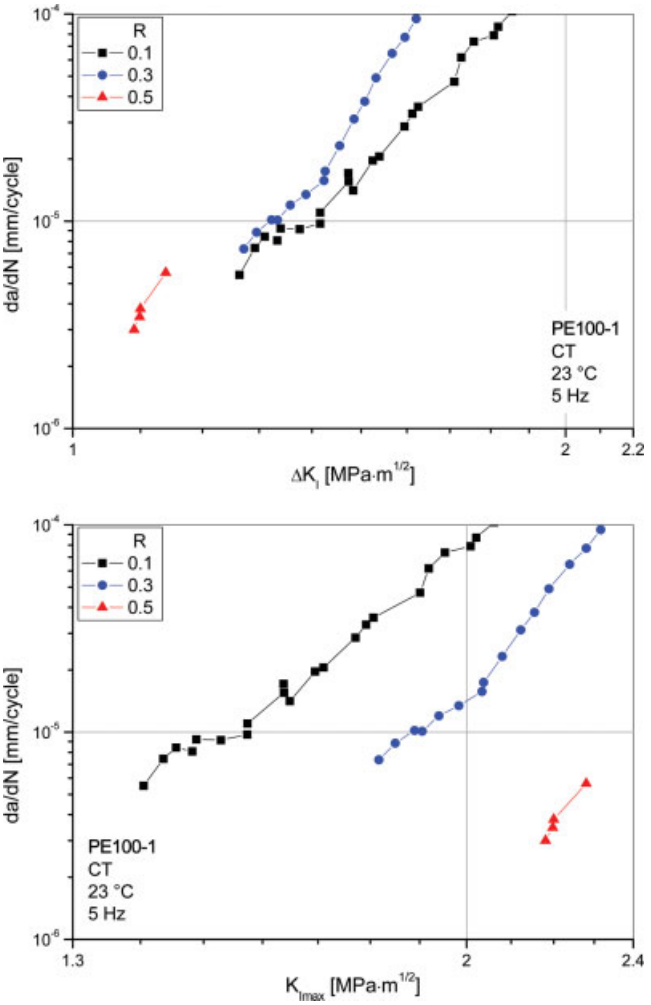

Figure 10 FCG rates in PE100-1 as a function of ΔK_I and K_{Imax}, using CT specimens and various R-ratios (23°C, 5 Hz). [Color figure can be viewed in the online issue, which is available at www.interscience.wiley.com.]

Optical micrographs of cross-sections of the process zone in PE100-1 are presented in Figure 11. In regions of plane stress, near the side surface of the specimen (normalized thickness, y/B = 0 and 0.05), the formation of a wedge-shaped process zone ahead of the crack was typical, as a result of crazing mechanisms. Under plane strain conditions (y/B ≈0.25 and 0.5),

TABLE II
Time to Failure, t_f, for FCG Investigations on PE100-1 at Various R-Ratios Using CT and CRB Specimens (23°C, R = 0.1)

	R	ΔK_{I0} [MPam$^{1/2}$]	$K_{Imax,0}$ [MPam$^{1/2}$]	t_f [h]
CT	0.1	1.2	1.3	37.2
	0.3	1.1	1.6	43.5
	0.5	1.0	2.0	41.6
CRB	0.1	0.75	0.8	18.9
	0.3	0.75	1.1	20.3
	0.5	0.75	1.5	1.0

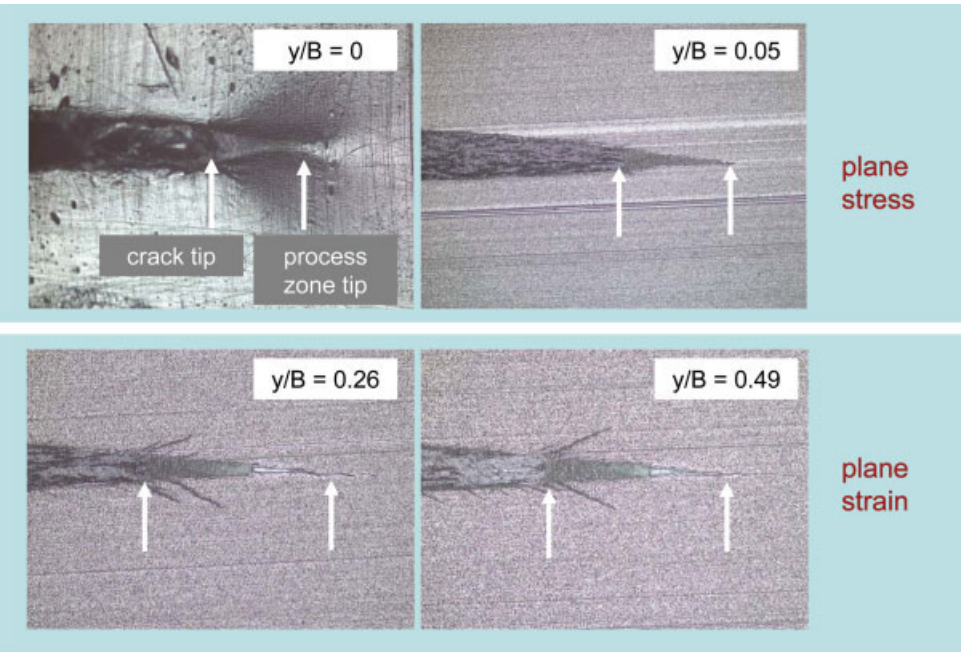

Figure 11 Fatigue crack profiles of PE100-1 under plane stress and plane strain conditions (23°C, 5 Hz, R = 0.1, ΔK_I = 1.6 MPa·m$^{1/2}$). [Color figure can be viewed in the online issue, which is available at www.interscience.wiley.com.]

additional side arms were detected at angles above and below this craze. These were not investigated in more detail, but are similar in appearance to shear crazes found in investigations with medium-density polyethylene (PE-MD) pipe grades.[24,35–37]

Corresponding to Figure 11, the crack front and the process zone front are shown in Figure 12. While the first half of the data presented was measured directly in the area $0 \leq y/B \leq 0.5$, the second half ($0.5 < y/B \leq 1$) was gained by duplicating and mirroring the experimental data. The front had an (almost) semi-elliptical shape over the entire cross-section. While the crack propagated faster in the middle of the specimen where it was exposed to plane strain conditions, retarded crack growth was found in side surface regions where plane stress conditions existed.

In addition, the process zone sizes measured using the cutting procedure (cross-sections) were compared with the step lengths of two neighboring striations at the fracture surface measured using scanning electron microscopy. The SEM examination was generally difficult, especially at higher values of ΔK_I where the striations could not be easily detected on the micrographs due to the increasingly indistinct appearance of the microstructure details. Keeping in mind the inaccuracy of both techniques, similar values were found in the cross-sections and at the fracture surfaces. It can be concluded that, under the test conditions selected, in each step of discontinuous crack propagation the crack jumps through the entire process zone. This is in good agreement with investigations on PE-MD,[24] where some variations in crack propagation modes, that depend on various test parameters (R-ratio, temperature, stress intensity factor), are discussed in more detail. Furthermore, the comparison strengthens the assumption that the drop in the process zone front in the middle of the specimen results from the inaccuracy of the measurement technique. This explanation sounds reasonable since no such drop was found in the corresponding striations at the fracture surface.

It is important to note that in all investigations presented here, the maximum of the process zone length, r_p, was always found in the middle of the CT speci-

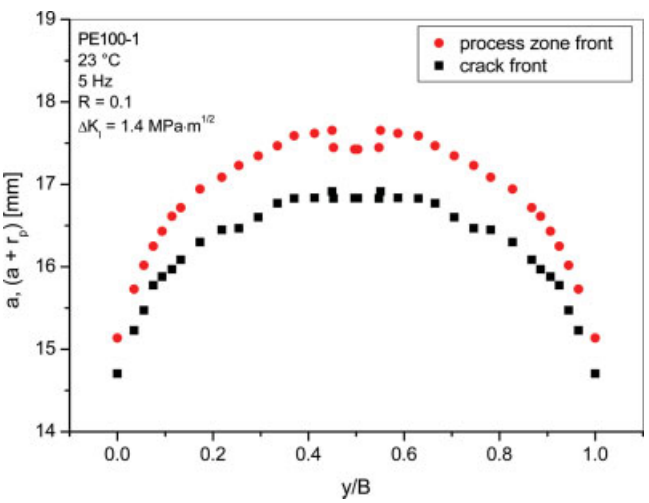

Figure 12 Crack front and process zone front in cyclically loaded PE-HD. [Color figure can be viewed in the online issue, which is available at www.interscience.wiley.com.]

men (i.e., under plane strain conditions). This goes against classical crack tip plastic zone models,[38] such as the ''dog bone model,'' where the largest process zone dimensions are associated with plane stress conditions. Similar results to the work presented in this report have been found in unpublished work at the Polymer Competence Center Leoben (PCCL) during the crack initiation period of crack propagation tests with PE pipe materials under static loading conditions. Hence, one idea to explain these facts is a phenomenological interpretation of the discontinuous crack growth mechanism (see Fig. 1); that is, in every crack growth step, process zone development in front of the crack may be understood as a crack initiation period. For a detailed explanation, more information about the local strain/stress conditions is necessary.

FCG tests with the same test parameters (R = 0.1, 5 Hz) were interrupted at three different values of ΔK_I (K_{Imax}) to study the effect of the stress intensity factor on process zone dimensions. In accordance with crack tip plastic zone models,[27,34,38] higher values of r_p were measured with an increase in stress intensity factor, while no changes in the shape of the process zone length distribution were observed. Because the maximum stress intensity factor, K_{Imax}, is assumed to have the most influence on the process zone dimensions under cyclic loading conditions,[27] Figure 13 shows r_p values of PE100-1 in terms of K_{Imax} for plane strain and plane stress conditions (FCG tests at 5 Hz). In the double-logarithmic graph, the measuring points are compared with fitted curves with a slope of 2 in accordance with many plastic zone models. The good correlation of these data sets confirms the assumption that process zone dimensions are frequently proportional to the ratio of the stress intensity factor to the relevant plastic deformation stress level (yield stress, σ_{ys}, or craze stress, σ_c).[38,39]

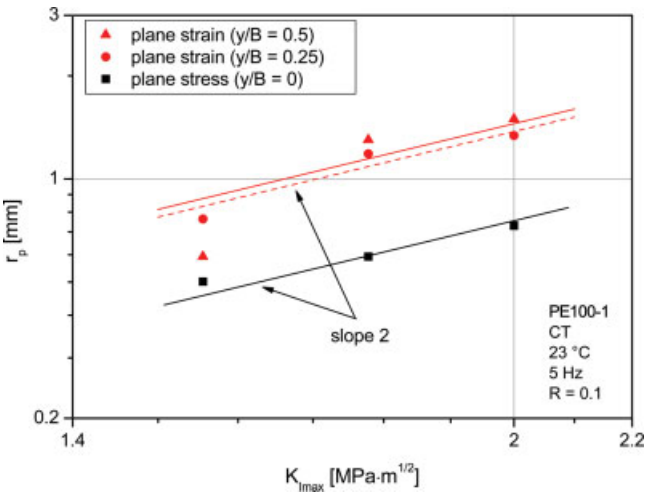

Figure 13 Effect of the maximum stress intensity factor K_{Imax} on the process zone length for PE 100-1. [Color figure can be viewed in the online issue, which is available at www.interscience.wiley.com.]

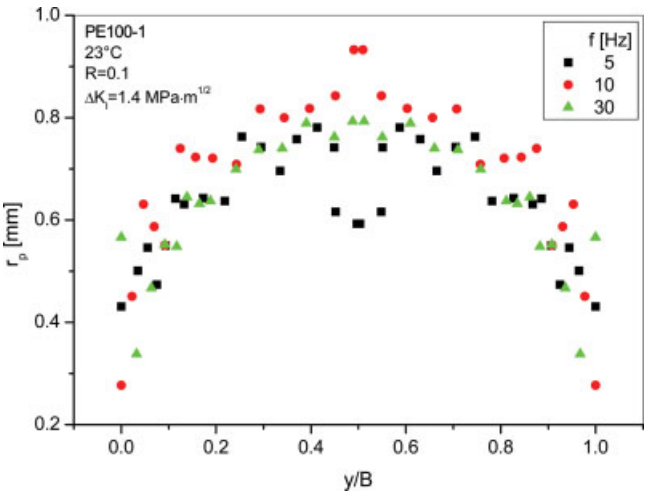

Figure 14 Effect of frequency on the process zone length during FCG in PE100-1 ($\Delta K_I = 1.4$ MPa $\cdot$ $m^{1/2}$). [Color figure can be viewed in the online issue, which is available at www.interscience.wiley.com.]

To investigate the effects of frequency on process zone development, FCG tests were conducted using CT specimens of PE100-1 at 5, 10, and 30 Hz and interrupted at three different values of ΔK_I (1.4, 1.6, and 1.8 MPa·$m^{1/2}$). The results of the through-thickness characterization of the process zone length are presented in Figure 14 for a ΔK_I value of 1.4 MPa·$m^{1/2}$. In summary, the influence of frequency on the process zone length was not significant. Differences found at a ΔK_I value of 1.6 MPa·$m^{1/2}$ can be explained as a result of two effects: (1) inaccuracy of measurement and (2) scatter band of the interruption point, which is illustrated by the wide region of interest for the through-thickness characterization in Figure 1 (stage 1). These results are in good correlation with the FCG kinetics, where no significant differences in FCG rates were found at ΔK_I values greater than approximately 1.4 MPa·$m^{1/2}$ (cf. Fig. 4).

As already shown in Figure 11, side arms were detected in the middle of the CT specimen (i.e., under plane strain conditions). Because of the density of data recorded in these investigations, the first appearance of such side arms could be detected in a narrow window in the thickness direction expressed as y/B. Side arms first appeared in the $0.03 \leq y/B \leq 0.15$ region. While these analyses resulted in tendentiously marginally smaller values at 5 Hz, no differences were observed between the results of the 10 Hz and 30 Hz tests. Generally, it can be concluded that the first appearance of side arms in the thickness direction values did not significantly depend on frequency under the test conditions selected.

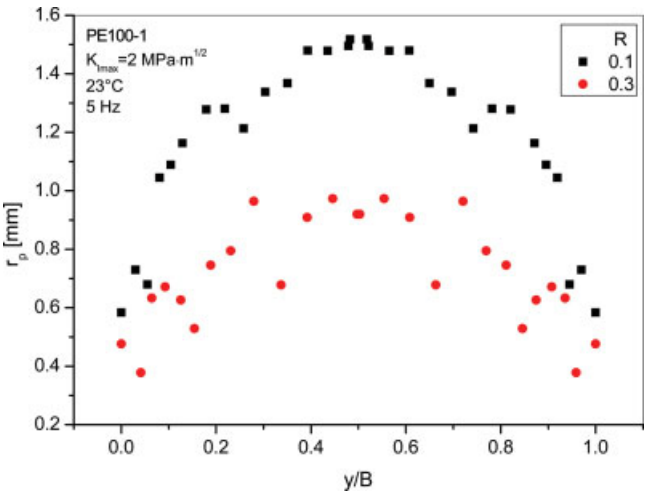

Figure 15 Effect of the R-ratio on the process zone length during FCG in PE100-1 (K_{Imax} = 2 MPa.m$^{1/2}$). [Color figure can be viewed in the online issue, which is available at www.interscience.wiley.com.]

The effect of the R-ratio on the process zone size is shown for PE 100-1 in Figure 15. The FCG tests were performed at R-ratios of 0.1 and 0.3 and a frequency of 5 Hz and interrupted at 3 different K_{Imax} levels (1.8, 2 and 2.2 MPa·m$^{1/2}$). In all three cases, the results were analogous to those shown in Figure 15 (K_{Imax} = 2 MPa·m$^{1/2}$): Longer process zone lengths were observed at the lower R-ratio. Although some inaccuracy of measurements must be taken into account, these results are contrary to the assumption that process zone dimensions are equal at constant K_{Imax} values.[19,34] In addition, smaller side arms occurred at the higher R-ratio. While the effect of the R-ratio on the process zone length is not yet clarified in detail, it is important to repeat the comment on the clear difference in the crack growth mechanism found in these investigations (cf. Fig. 8). An R-ratio of 0.1 lead to a discontinuous crack propagation, at higher R-ratios a change of crack growth mode from discontinuous to continuous crack propagation was found.

Calculation of the effective crack length

The calculation of the effective crack length was based on Eq. (1) for the dynamic modulus, E_{dyn}, where ΔF is the range of the applied load, ΔCOD_0 the range of crack opening displacement (measured at the front face of the specimen) and $V_0(a/W)$ a correction term for the CT specimen [see Eq. (2)].[40] E_{dyn} was assumed to be constant for the entire FCG test cycle (method 1). It is important to note that E_{dyn} was determined using the initial crack length (i.e., razor blade pre-crack), before crack initiation and crack propagation could take place. Crack opening displacement (COD) was measured using an extensometer at the front face of the CT specimen:

$$E_{dyn} = \frac{\Delta F}{\Delta COD_0 \cdot B} \cdot V_0\left(\frac{a}{W}\right) \quad (1)$$

$$V_0\left(\frac{a}{W}\right) = \left(1 + \frac{0.25}{\frac{a}{W}}\right) \cdot \left(\frac{1+\frac{a}{W}}{1-\frac{a}{W}}\right)^2 \cdot \left[1.6137 + 12.6784 \cdot \frac{a}{W} - 14.231 \cdot \left(\frac{a}{W}\right)^2 - 16.61 \cdot \left(\frac{a}{W}\right)^3 + 35.05 \cdot \left(\frac{a}{W}\right)^4 - 14.494 \cdot \left(\frac{a}{W}\right)^5\right] \quad (2)$$

In addition, these data were compared with mean crack length values, a_m and $(a + r_p)_m$ calculated assuming equal fracture surface areas (method 2, cf. Fig. 16). In contrast to a_m, the determination of $(a + r_p)_m$ was based on various crack tip plastic zone models, where process zone length is considered part of the effective crack length.[38,39] Although a volumetric calculation would be preferable, a simple two-dimensional approach (which is a mathematical simplification of the physical reality) was taken to check the validity of the defined methodology in a first rough estimation. An overview of the two methods used for the determination of effective crack length is given in Figure 17.

The results of effective crack length calculation are presented in Figure 18 in comparison with the measured data (i.e., crack front and process zone front) for the FCG test at 23°C, an R-ratio of 0.1 and a frequency of 5 Hz that was interrupted at a $\Delta K_{I,int}$ value of 1.4 MPa·m$^{1/2}$. The effective crack length was in the range between the maximum crack length, a_{max}, and the maximum crack length including process zone length $(a + r_p)_{max}$. The good agreement of the various effective lengths based on both the compliance relationship and equal area of fracture surface models confirms

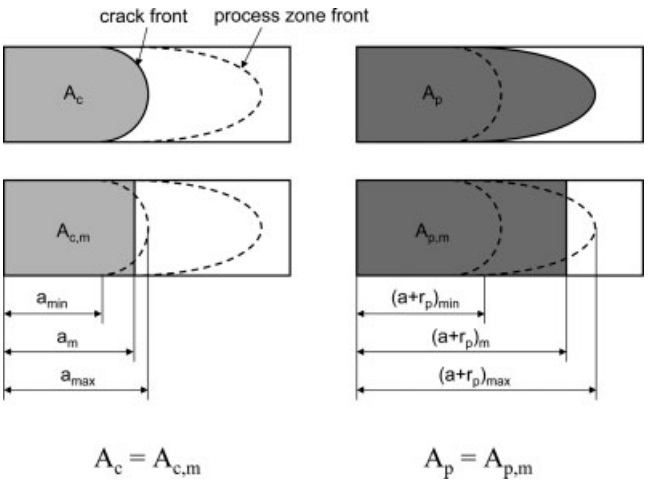

Figure 16 Overview of various crack length values at the fracture surface.

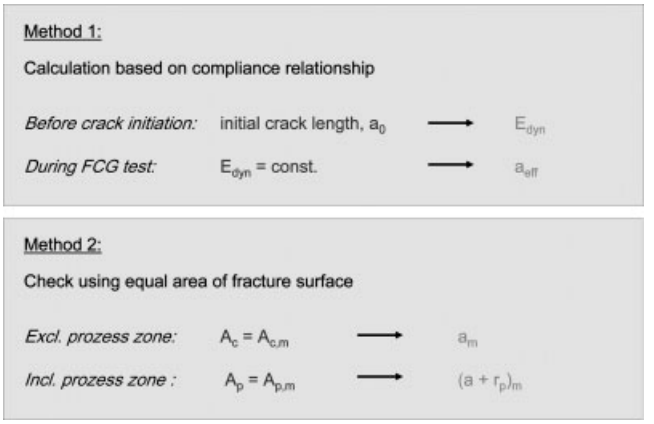

Figure 17 Methods for calculation of effective crack length data.

the assumption taken, especially when a_{eff} and $(a + r_p)_m$ are compared. The same situation was found for the interrupted FCG tests at $\Delta K_{I,int}$ values of 1.6 and 1.8 MPa·m$^{1/2}$.

Figure 19 shows a method of comparing the calculated crack length data with some particular measured crack lengths in a more compact way, where the dynamic modulus is shown for the normalized crack lengths, a/W and $(a+r_p)/W$. The latter value includes the process zone length. From an experimental point of view, the following crack length values are interesting when using optical devices for the determination of crack length during FCG testing: a_{min}, $(a+r_p)_{min}$, a_{max} and $(a+r_p)_{max}$.

Figure 19 presents an overview of this special analysis of FCG tests performed at 23°C with an R-ratio of 0.1 and a frequency of 5 Hz. The tests were interrupted at $\Delta K_{I,int}$ values of 1.4, 1.6, and 1.8 MPa·m$^{1/2}$. It is not surprising that the crack length minima measured optically (i.e., a_{min} and $(a+r_p)_{min}$) led to an underestimation of the dynamic modulus, while E_{dyn}

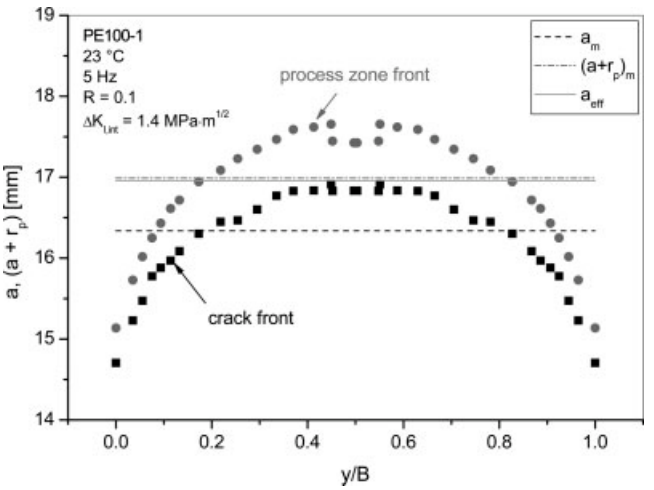

Figure 18 Comparison of crack length measurements and calculated crack length data ($\Delta K_{I,int}$ = 1.4 MPa.m$^{1/2}$).

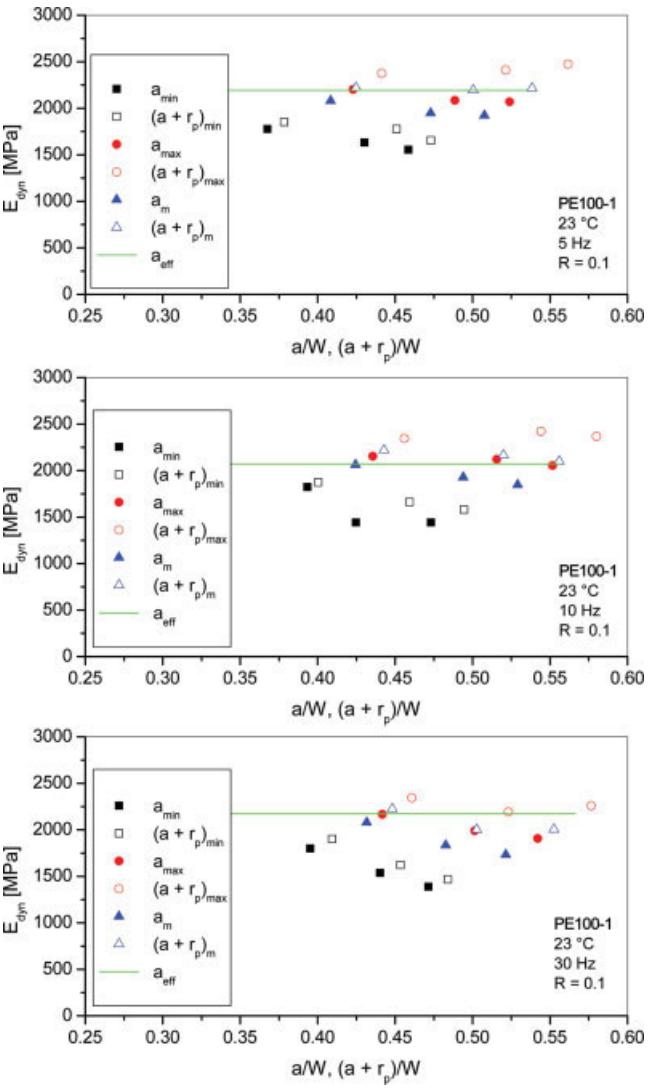

Figure 19 Calculation of E_{dyn} values using various crack length data at three different frequencies (5, 10, and 30 Hz). [Color figure can be viewed in the online issue, which is available at www.interscience.wiley.com.]

was overestimated by using the crack length maxima (i.e., $(a+r_p)_{max}$). The conclusion drawn from these results is that not all crack length data measured using commercial optical equipment agree satisfactorily with the effective crack length calculated based on compliance relationships. The best correlation was found between a_{eff}, $(a + r_p)_m$ and a_{max} values. Unfortunately, with regard to a_{max}, the problem is that experimental determination using the optical microscope is difficult, if not impossible.

The effective crack lengths calculated based on compliance relationships are shown as a function of the cycle number, N, in Figures 20 and 21. The stepwise curves in Figure 20 document the discontinuous crack growth at all three frequencies. Differences in crack growth mechanisms are clearly obvious in Figure 21. While discontinuous crack growth is the predominant mechanism in the case of an R-ratio of 0.1

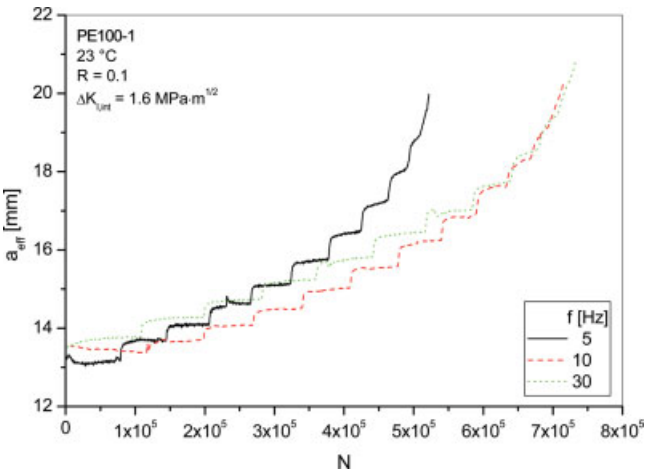

Figure 20 Effective crack length curves at various frequencies (5, 10, and 30 Hz). [Color figure can be viewed in the online issue, which is available at www.interscience.wiley.com.]

(as documented by the stepwise curve), a transformation from discontinuous to continuous crack growth was observed at an R-ratio of 0.3. This reflects well the results presented above and is also in good agreement with investigations presented previously.[24] In general, it can be concluded that calculating the effective crack length based on compliance relationships is a powerful tool with two main advantages. First, it allows a dense determination of crack length values that are characteristic for the crack growth mechanism (continuous or discontinuous), as discussed above. Satisfactory results (including high reproducibility) are obtained with some effort in test device and test procedure (e.g., use of extensometer). Second, in comparison with the ISO standard for fatigue testing of PE,[41] the fatigue test approach presented here allows an easier handling. No additional tensile tests are necessary to obtain modulus data, but all values are easily determined in one and the same FCG experiment. Furthermore, no regression coefficients are needed to calculate the effective crack length.

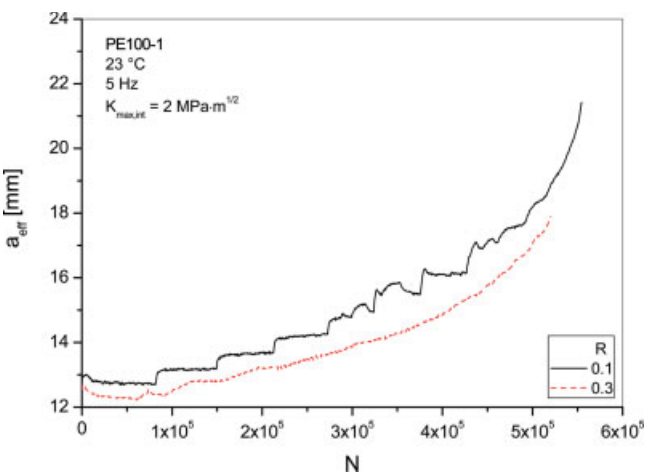

Figure 21 Differences in crack growth mechanisms for different values of R-ratio (0.1 and 0.3). [Color figure can be viewed in the online issue, which is available at www.interscience.wiley.com.]

FCG modeling

In principle, information on the crack length function in the thickness direction allows the crack growth kinetics data experimentally determined for a certain position in the thickness direction to be used to calculate the crack growth kinetics data for any other position in the thickness direction. In other words, it is possible to model FCG rates in the middle of the CT specimen based on data obtained at the side surface of the CT specimen.

Fatigue crack propagation in PE100-1 has been investigated in detail by determining all FCG rates at the side surface of the CT specimen. It is important to note that the crack length included the process zone. To manage the calculation of data for the center of the CT specimen, the difference between a_{max} and $(a + r_p)_{min}$ was determined at various $\Delta K_{I,int}$ levels, as shown, for example, in Figure 22 (23°C, R = 0.1). While the scatter band of these results has not been investigated in more detail, a fit of the data, based on Equation 3 (with two coefficients, C_1 and C_2), was used to calculate data for the middle of the CT specimen from the basic data sets:

$$a_{max} - (a + r_p)_{min} = C_1 + \frac{C_2}{\ln \Delta K_I((a + r_p)_{min})} \quad (3)$$

The results of the modeling are summarized in Figure 23 for FCG tests at different frequencies, where the FCG rates are shown as a function of the stress in-

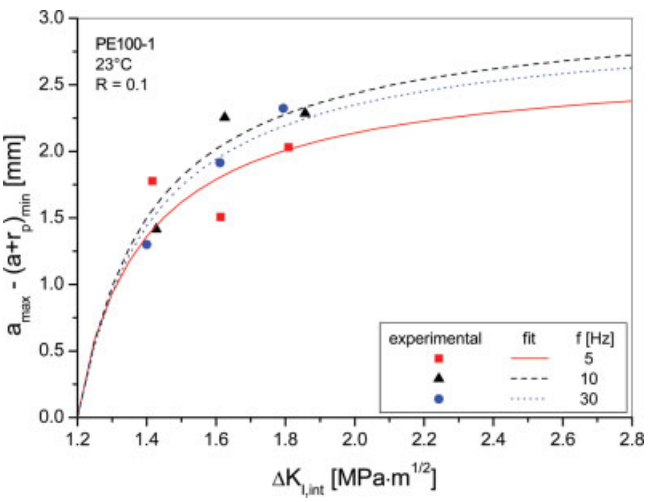

Figure 22 Calibration curve for the calculation of FCG rates in the middle of the CT specimen based on data measured at the specimen side surface. [Color figure can be viewed in the online issue, which is available at www.interscience.wiley.com.]

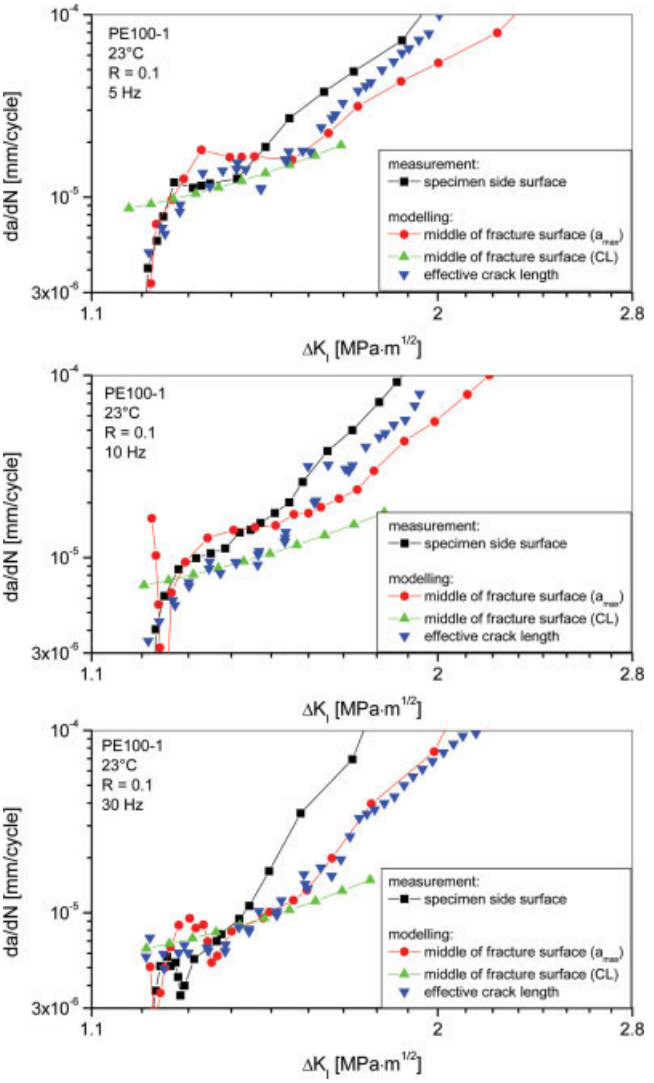

Figure 23 Results of the modeling of FCG tests at different frequencies (5, 10, and 30 Hz). [Color figure can be viewed in the online issue, which is available at www.interscience.wiley.com.]

tensity factor range. In comparison with the results at the side surface of the CT specimen, FCG rates in the middle of the CT specimen are shifted to the right. Furthermore, they are in good agreement with results obtained based on the crack layer theory, where crack propagation in the middle of the specimen was also modeled.[42] As expected, FCG rates determined using the effective crack length lie between the other curves.

SUMMARY AND CONCLUSIONS

Comprehensive information was gained about the FCG kinetics and the development of process zones at the crack tip in a PE-HD pipe material varying important test parameters such as specimen configuration, frequency, and R-ratio. While CT testing seems to be more convenient for studying the details of FCG kinetics, CRB testing allows a significant reduction of testing time and is a powerful tool for ranking materials in terms of failure time. The calculation of effective crack length based on compliance relationships represents a very useful alternative to the optical determination of crack length data. It is based on polymer-physical principles and allows us to gain detailed information about both the fatigue mechanisms and FCG kinetics.

The research work for this article was performed at the Polymer Competence Center Leoben GmbH (PCCL, Austria) within the framework of the K_{plus}-program of the Austrian Ministry of Traffic, Innovation and Technology with contributions by the Institute of Materials Science and Testing of Plastics (University of Leoben, A) and Dow Chemical (Horgen, CH).

References

1. Kramer, E. J.; Berger, L. L. In Advances in Polymer Science—Crazing in Polymers; Kausch, H.-H., Ed.; Springer: Berlin, 1990; p 1.
2. Kausch, H.-H. In Failure of Plastics; Brostow, W.; Corneliussen, R. D., Eds.; Hanser: Munich, 1986; p 84.
3. Ramsteiner, F. In The Application of Fracture Mechanics to Polymers, Adhesives and Composites; Moore, D. R., Ed.; Elsevier: Oxford, UK, 2004; p 31.
4. Lang, R. W.; Stern, A.; Dörner, G. Angew Makromol Chem 1997, 247, 131.
5. Pinter, G. PhD Thesis, Institute of Materials Science and Plastics Testing, University of Leoben, Leoben (A), 1999.
6. Pinter, G.; Haager, M.; Wolf, C.; Lang, R. W. Macromol Symp 2004, 217, 307.
7. Men, Y. F.; Rieger, J.; Enderle, H.-F.; Lilge, D. Eur Phys J E 2004, 15, 421.
8. Song, M. M.; Hu, G. X.; Hu, L. J. Polym Test 1998, 17, 311.
9. Fleissner, M. Kunststoffe 1987, 77, 45.
10. Williams, J. G. Fracture Mechanics of Polymers; Ellis Horwood: Chichester, UK, 1987.
11. Hertzberg, R. W.; Manson, J. A. Deformation and Fracture Mechanics of Engineering Materials; John Wiley & Sons: New York, 1989.
12. Lang, R. W.; Pilz, G.; Pinter, G.; Stern, A. Plastics Spec 2000, 6, 26.
13. Laurent, E. In Conf. Proc. Plastic Pipes XI, Munchen D, 2001, 11, 63.
14. Dörner, G.; Lang, R. W. 3R Int 1997, 36, 672.
15. Pinter, G.; Lang, R. W. In The Application of Fracture Mechanics to Polymers, Adhesives and Composites; Moore, D. R., Ed.; Elsevier: Oxford, UK, 2004; p 47.
16. Kasakevich, M. L.; Moet, A.; Chudnovsky, A. Polymer 1991, 31, 435.
17. Reynolds, P. T.; Lawrence, C. C. J Mater Sci 1991, 26, 6197.
18. Kadota, K.; Chum, S.; Chudnovsky, A. J Appl Polym Sci 1993, 49, 863.
19. Pinter, G.; Balika, W.; Lang, R. W. In Temperature–Fatigue Interaction; Remy, L.; Petit, J., Eds.; Esis: Amsterdam, the Netherlands, 2002; p 267.
20. Zhou, Y.-Q.; Brown, N. J Polym Sci Part B: Polym Phys 1992, 30, 477.
21. Reynolds, P. T.; Lawrence, C. C. J Mater Sci 1993, 28, 2277.
22. Lawrence, C.; Teo, S.; Potter, R. In Conf. Proc. at Plastics Pipes X, Göteborg (S), September 14–17, 1998; p 743.

23. Chudnovsky, A.; Shulkin, Y.; Baron, D.; Lin, K. P. J Appl Polym Sci 1995, 56, 1465.
24. Parsons, M.; Stepanov, E. V.; Hiltner, A.; Baer, E. J Mater Sci 2000, 35, 2659.
25. Pinter, G.; Haager, M.; Balika, W.; Lang, R. W. Plast Rubber Compos 2005, 34, 25.
26. Favier, V.; Giroud, T.; Strijko, E.; Hiver, J. M.; G'Sell, C.; Hellinckx, S.; Goldberg, A. Polymer 2002, 43, 1375.
27. Lang, R. W. PhD Thesis, Lehigh University, Bethlehem, PA, 1984.
28. Parsons, M.; Stepanov, E. V.; Hiltner, A.; Baer, E. J Mater Sci 2000, 35, 1857.
29. Yngvesson, M. Int J Fract 2000, 102, L9.
30. Pinter, G.; Haager, M.; Lang, R. W. Polym Test 2006 (in press).
31. Haager, M.; Pinter, G.; Lang, R. W. In Conf. Proc. Antec 2006, Charlotte, NC, May 7–11, 2006.
32. Bucknall, C. B.; Dumpleton P. Plast Rubber Proc Appl 1985, 5, 343.
33. Parsons, M.; Stepanov, E. V.; Hiltner, A.; Baer, E. J Mater Sci 1999, 34, 3315.
34. Lang, R. W.; Balika, W.; Pinter, G. In The Application of Fracture Mechanics to Polymers, Adhesives and Composites; Moore, D. R., Ed.; Elsevier: Oxford, UK, 2004; p 83.
35. Parsons, M.; Stepanov, E. V.; Hiltner, A.; Baer, E. J Mater Sci 2001, 36, 5747.
36. Strebel, J. J.; Moet, A. J Mater Sci 1991, 26, 5671.
37. Strebel, J. J.; Moet, A. J Polym Sci Part B: Polym Phys 1995, 33, 1969.
38. Saxena, A. Nonlinear Fracture Mechanics for Engineers; CRC Press: Boca Raton, FL, 1998.
39. Anderson, T. L. Fracture Mechanics—Fundamentals and Applications; CRC Press: Boca Raton, FL, 1991.
40. Saxena, A.; Hudak, S. J. Int J Fract 1978, 14, 453.
41. ISO 15850, 2002.
42. Balika, W.; Pinter, G.; Choi, B.-H.; Lang, R. W. In Conf. Proc. Antec 2004, Chicago, IL, May 16–20, 2004; p 4028.